heritage

MDPI

Article

Study of the Patinas of an Outdoor Bronze Statue "Cesare Augusto" in Brindisi (Southern Italy)

Giovanni Buccolieri [1], Antonio Serra [1], Elisabetta Palmiero [2], Fabio Paladini [1], Gianluca Bozzetti [3], Alfredo Castellano [1] and Alessandro Buccolieri [1,*]

[1] Dipartimento di Matematica e Fisica "E. De Giorgi", University of Salento, 73100 Lecce, Italy; giovanni.buccolieri@unisalento.it (G.B.); antonio.serra@unisalento.it (A.S.); fabio.paladini@unisalento.it (F.P.); alfredo.castellano@unisalento.it (A.C.)
[2] Restauratrice dell'Azienda Colaci Emilio Impianti e Restauri, Alessano, 73031 Lecce, Italy; prorestauro@libero.it
[3] Fondazione Nuovo Teatro Verdi, 72100 Brindisi, Italy; gianlucabozzetti@gmail.com
* Correspondence: alessandro.buccolieri@unisalento.it

Abstract

The aim of this paper is the analysis of the main elements of the patinas of an outdoor bronze monument by using portable energy-dispersive X-ray fluorescence (ED-XRF) equipment designed and assembled at the University of Salento. Thanks to the versatility of the ED-XRF portable apparatus, we carried out a scan based on a limited set of measurements that was representative of the studied surface of the monument before the restoration in a relatively short time and in a completely non-invasive way. We investigated the concentrations of copper, zinc, lead, chlorine, iron, tin and sulphur in the statue dedicated to the emperor Caesar Augustum, which was created in 1935 and later placed in Brindisi (Apulia, Southern Italy). Moreover, X-ray diffraction (XRD) and Raman spectroscopy were carried out for a sample of patina in order to identify its chemical composition. The information obtained can be helpful for restoration work on this statue and possible future monitoring.

Keywords: outdoor statue; bronze; patina; portable ED-XRF; XRD; Raman

1. Introduction

Bronze artefacts are important relics of our historical and artistic heritage that are susceptible to degradation processes in indoor environments such as museums [1], and especially when they are exposed to aggressive outdoor atmospheres (for example, industrial or marine areas) [2] and when they are found buried in soil or on the seabed [3,4].

Outdoor bronze statues interact with air pollutants to form corrosion products [5–7], resulting in patinas of various colours (for example, red, green, brown, and black), as well as imperfections and cracks [8–10].

It is known that the chemical composition of the patinas of outdoor bronze artefacts depends on multiple factors, such as the nature of the alloy, porosity, atmospheric pollutants (sulphur dioxide, nitrogen oxide and ozone), acid rain [11], variations in humidity and temperature, the colonization of microorganisms and ultraviolet radiation [12,13]. All of these factors contribute to the formation of unstable copper oxychloride compounds that cause both esthetic and structural damage to the artefact [14,15].

Academic Editor: João Pedro Veiga

Received: 8 April 2026
Revised: 26 June 2026
Accepted: 28 June 2026
Published: 7 July 2026

In particular, the dominant corrosion factors in areas with large industrial ports in a maritime and industrial environment are primary and secondary marine aerosols and anthropogenic combustion products (particulate and gaseous) [16].

The determination of the chemical composition of the alloy of a bronze object is important for various reasons, such as, for example, to highlight any degradation products [17], and to help restorers in subsequent conservation work, as well as to discover the manufacturing technique [18], estimate the effectiveness of protective coatings and/or corrosion inhibitors before and after restoration work [19], and evaluate the authenticity of the object [20].

Various analytical techniques, both destructive and non-destructive, can be used to study ancient or more modern bronze artefacts [21–23], and the results obtained are often processed using multivariate statistical techniques [24,25] and simulation databases [26].

The aim of this research is to determine the main elements of the patinas on an outdoor bronze monument using portable energy-dispersive X-ray fluorescence (ED-XRF) equipment.

We investigated the concentrations of copper, zinc, lead, chlorine, iron, tin and sulphur on the patinas of a bronze statue dedicated to Cesare Augusto, which was created in 1935 and later placed in Brindisi (Apulia, Southern Italy).

Thanks to the versatility of the ED-XRF portable apparatus, we carried out a scan of the monument before the restoration, in a relatively short time, based on a limited set of measurements, but representative of the studied surface of the statue. This allowed us to obtain valuable information, since the chemical characterization of the surface layer of a monument is an essential preliminary phase for the subsequent restoration, cleaning and conservation of the statue. Moreover, X-ray diffraction (XRD) analysis and Raman spectroscopy were carried out on a sampled patina to determine its chemical composition. In fact, the primary modification suffered by a bronze alloy is the chemical–physical formation of new mineral species (corrosion products). These compounds can be stable and protect the bulk from a deeper corrosion (as copper hydroxycarbonates) or can further react once the external environmental conditions have changed (as copper chlorides) [27].

2. Materials and Methods

2.1. Description of the Site

Brindisi has played an important commercial, industrial, and cultural role over the centuries, thanks to its location in Apulia (Southern Italy) along the Adriatic Sea and in the centre of the Mediterranean Sea. Figure 1 shows the location of Brindisi and where the studied statue is located.

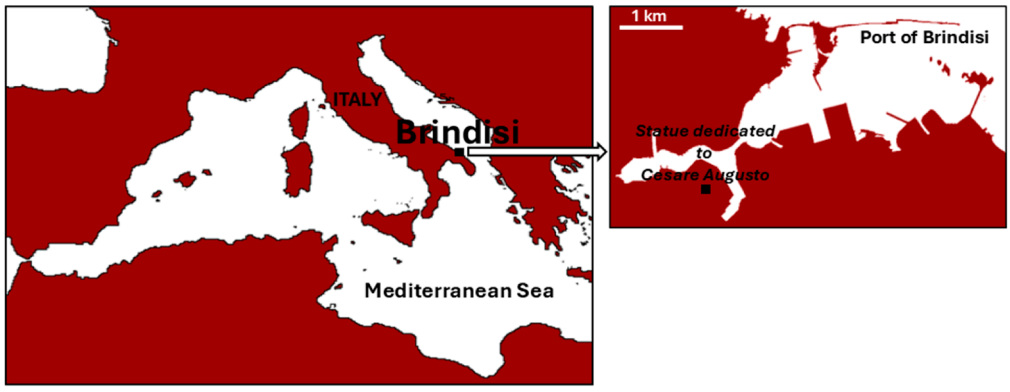

Figure 1. Location of Brindisi (Apulia, Southern Italy) and of the statue studied.

From September 1943 to February 1944, Brindisi was the provisional seat of government of the Kingdom of Italy.

Brindisi has approximately 81,000 residents and it is characterized by warm, arid summers and mild winters.

For many years, Brindisi was an important centre for the chemical and thermoelectric industries, becoming one of the most highly industrialized cities in Southern Italy [28]. Fifteen kilometres from Brindisi, there is one of the largest coal-fired power plants in Europe, currently inactive. However, in recent years, a transition toward more sustainable energy sources and a green economy has been underway.

The port of Brindisi is crucial for trade, tourism, transportation, and logistics, handling cargoes such as coal, oil, natural gas, and chemicals [29].

The strategic position of the airport in the Mediterranean region, along with its natural potential for multi-modal (the port is a few kilometres away) operations, have made it a base of crucial importance for both national defence and NATO. Since 2000, Brindisi has been the site of the United Nations Humanitarian Response Depot (UNHRD).

2.2. Description of the Statue

The object of this study is an outdoor bronze statue that was created in 1935, but the origin of the raw materials used for the building of the monument is not known. Figure 2 shows two photos of the studied manufact. The statue is 310 cm tall, and it is supported on a 19 cm high bronze base (96 × 92 cm) and on a 191 cm high stone base. This monument, depicting Emperor Caesar Augustus, is in Brindisi in the Piazza del Popolo. It is surrounded to the east, north and west by the sea, about 300 m away from it.

Figure 2. Photos of the front (**a**) and left side (**b**) of the outdoor bronze statue dedicated to the emperor Caesar Augustus located in the Piazza del Popolo in Brindisi (Southern Italy).

The analysed artefact is a bronze copy of the famous marble original known as the Augustus of Prima Porta. This marble work was discovered in 1863–1864 inside the Villa of Livia, the emperor's consort, at Prima Porta in Rome, and it is currently housed in the Vatican Museums. The marble work dates to the Tiberian era (14–37 AD).

The bronze copy analysed in this work was created by the Chiurazzi Foundry, founded in 1870 in Naples, Italy. The Chiurazzi Foundry specialized in reproducing classical and Renaissance sculptures by using the lost-wax casting technique and producing casts of them. The foundry had a collection of over a thousand plaster casts of sculptures from the National Archaeological Museum of Naples, the Vatican Museums, the Capitoline Museums, the Borghese Museum in Rome, the Pitti Palace, the Uffizi Gallery, and the National Archaeological Museum of Florence.

The statue under study was created during preparations for the Augustan Bimillenary. Its significance is therefore intrinsically linked to the political and ideological contexts in which it was commissioned and installed. The work is a symbolic "double" that reproduces the iconography of the ancient emperor, but the historical life of which unfolds entirely within modern Italian history.

2.3. ED-XRF Analysis

Energy-dispersive X-ray fluorescence (ED-XRF) analyses were carried out using an apparatus designed and assembled at the University of Salento [30].

This portable tool is composed of the following components: an X-ray tube produced by MOXTEK® (Orem, UT, USA) with an anode of palladium operating at 1–40 kV of voltage and 0–100 μA of current, and a Si-PIN detector produced by AMPTEK® (Bedford, MA, USA), model XR_100CR, thermoelectrically cooled, with a beryllium window of 25 μm. The detector has a resolution of 150 eV at 5.9 keV and a resolution of about 250 eV in the range 10–15 keV and incorporates a pocket multi-channel analyser produced by AMPTEK® (Bedford, MA, USA), model MCA8000A, interfaced with a laptop. The measurements were taken not exactly in contact, but at about 2 mm from the surface of the statue. The diameter of the X-ray beam on the surface of the sample is an ellipse, the axes of which are equal to 2 mm and 3 mm.

Figures 3 and 4 show the measurement points of the ED-XRF analysis.

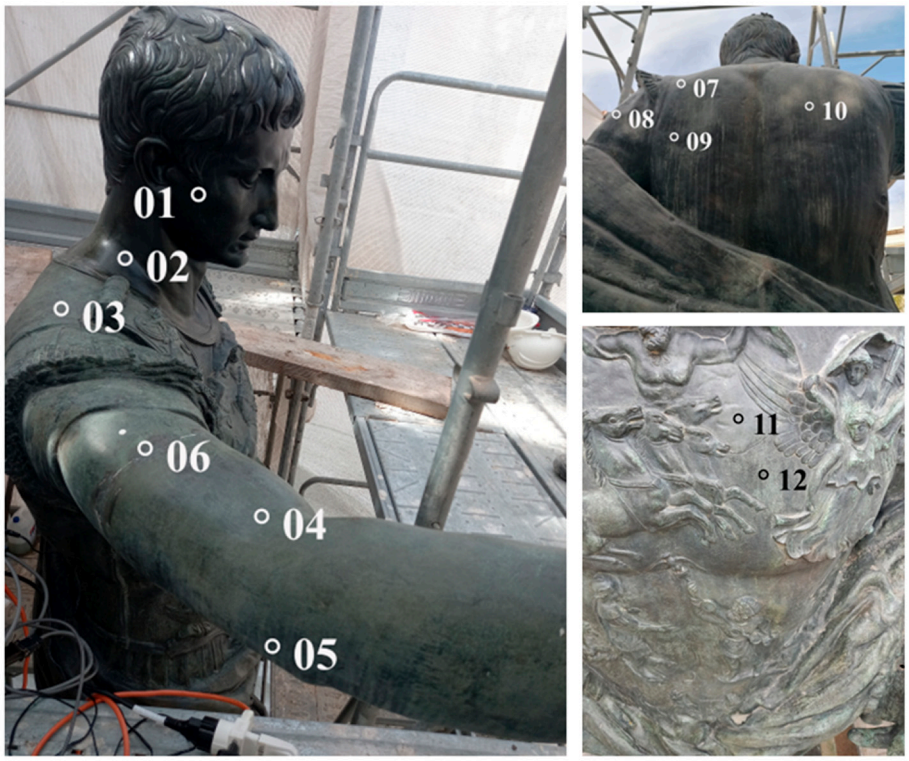

Figure 3. Measuring points on the upper part of the studied statue.

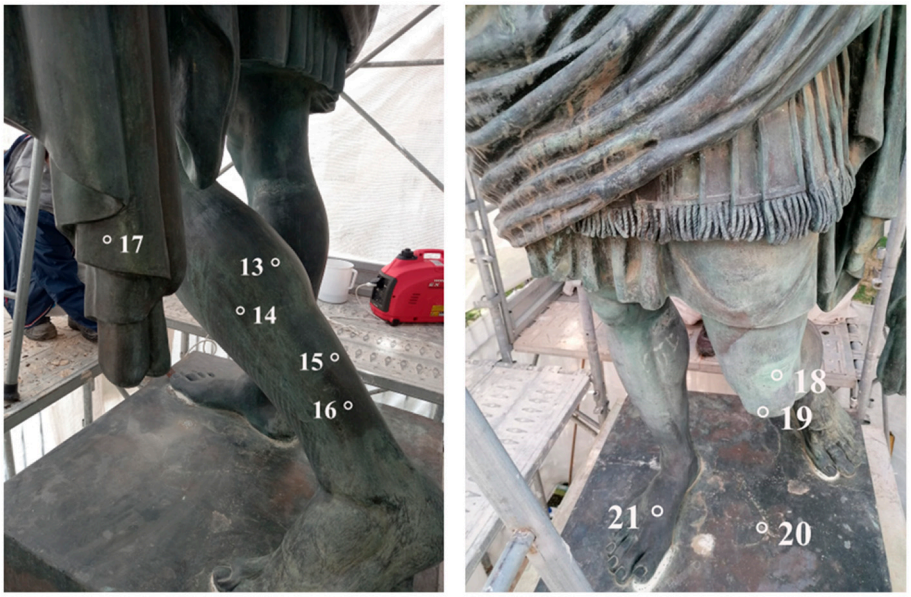

Figure 4. Measuring points on the lower part of the analysed statue.

Copper, zinc, lead and iron were quantitatively determined at high energy, specifically, 20 kV of voltage and 3 μA of current, with an acquisition time of 60 s, by using a 30 μm aluminium filter placed on the source, whereas chlorine, tin and sulphur were quantitatively determined at low energy, specifically, 6 kV of voltage and 40 μA of current, with an acquisition time of 60 s. These values were sufficient to excite by Bremsstrahlung radiation the lines for Cu-Kα (8.04 keV), Zn-Kα (8.64 keV), Pb-Lα (10.55 keV), Cl-Kα (2.62 keV), Fe-Kα (6.44 keV), Sn-Lα (3.44 keV) and S-Kα (2.31 keV).

The evaluation of the spectral interference between sulphur (K-line) and lead (M-line) is fundamental in the relevant ED-XRF quantitative investigation. The separation between the K-line of sulphur and M-line of lead is equal to about 40 eV, a value which is lower than the resolution of the detector (equal to about 150 eV). The separation of the two signals was obtained through the deconvolution of the peaks to solve this problem. This deconvolution is possible considering both the different concentrations and the different fluorescent yields between the two elements: K-line of sulphur (0.061) and M-line of lead (0.032) [31–33]. The software produced by Microcal Origin Professional® (Northampton, MA, USA) was used for deconvolution of peaks. The deconvolution was performed using Gaussian (version 2018) as the signal integration function:

$$y = y_0 + \frac{A}{w\sqrt{\frac{\pi}{2}}} e^{-\frac{2(x-x_c)^2}{w^2}} \quad (1)$$

where A is the signal intensity, x_c represents the signal energy to be integrated, y_0 is the background, and w is the FWHM (peak width at half-height). For each element investigated, the values of y_0, x_c and w were kept constant for both the calibration and analytical samples.

The calibration was carried out by analysing ten standards, consisting of Cu, Cu_2O, CuO, $CuCO_3$, Cu/Sn (80/20% *w*/*w*), Cu/Pb (80/20% *w*/*w*), Pb_3O_4, Zn, Fe, $CuCl_2$, $CuSO_4$ and SnO_2 in different ratios. The concentration of each standard was chosen to replicate the chemical composition of the investigated patinas. All chemical compounds were analytical grade and purchased from Sigma-Aldrich® (Milan, Italy), except the Cu/Sn (80/20% *w*/*w*) standard, which was purchased from Goodfellow® (Cambridge, UK).

Each standard was prepared by mixing the compounds in different weight percentages. Specifically, the chemical compounds were weighed using an analytical balance produced

by KERN® (Konolfingen, Switzerland), model ABT 100–5M, subsequently mixed and homogenized in an agate mortar for ten minutes and finally compressed at 200 bar for ten minutes using a laboratory press. The laboratory press compacts the powders into solid tablets, ensuring uniform dosages for subsequent analyses. The homogeneity of elements in the standard meets the requirements for the ED-XRF quantitative determination.

Additionally, the analysed samples are assumed to demonstrate infinite thickness [34,35], and the quantitative results are obtained, for each element, as a weight percentage (wt %).

The ED-XRF analyses involved thicknesses of patina of a few dozen micrometres, considering that a radiation between 5 and 10 keV, passing through 40 μm of cuprite, is attenuated by a factor of 100. The experimental data were elaborated by the software produced by Microcal Origin Professional®.

Table 1 summarizes the chemical composition of ten standards used in the ED-XRF quantitative analysis. The reported values indicate the percentages by mass (wt %) of the various elements in each standard.

Table 1. Percentages by mass (wt %) of the standards used in ED-XRF calibration.

N.	Cu	Zn	Pb	Cl	Fe	Sn	S	C	H	O
	(wt %)									
01	57.0	10.9	11.9		8.8	11.5				
02	63.7	8.8	6.0		4.3	7.2				10.0
03	55.1	5.0	8.9	3.8	4.9	10.8	3.2			8.2
04	41.8	3.8	5.5			19.1	9.7	0.7	0.1	19.1
05	29.0	1.9	2.7		7.6	29.4	4.0	1.3	0.2	24.0
06	31.3		8.6	5.1	11.5	25.8		0.9	0.1	16.7
07	38.4	6.3	4.8	2.5	10.3	12.7	7.1	0.8	0.1	17.0
08	72.2		8.7							19.1
09	58.1		23.9	1.7						16.3
10	88.1									11.9

2.4. XRD Analysis

An automatic diffractometer produced by Philips® (Malvern Panalytical, Hamburg, Germany), model PW3020 X'Pert, was used for the X-ray diffraction (XRD) examination of a sample of deposit collected from a part of the statue not exposed to water erosion. In particular, the sample was taken from an area not exposed to leaching, near the regions n. 15 and n. 16 (Figure 4), by using a bistoury. The primary purpose of the sampling was to verify the compounds and, particularly, the nature of the chlorides present on the statue. Experimental conditions were as follows: Cu-Kα radiation at 40 kV and 45 mA. The instrument was in a Bragg–Brentano configuration θ–2θ with scan step of 0.02°, at 0.2 mm receiving slit, 0.04 rad Soller slit, 1/2° divergence slit and 15 mm beam mask.

The experimental data were elaborated by the software produced by Profex (Solothurn, Switzerland), Open Source XRD and Rietveld Refinement version 5.6.

2.5. Raman Spectroscopy

Raman analysis was performed, on the same sample used for the X-ray diffraction analysis, to identify patina composition.

The sample was pounded to a fine powder in an agate mortar, homogenized and subsequently investigated. Raman analyses were achieved by using a spectrometer produced by Renishaw® (Wotton-under-Edge, UK), model Invia (spectral resolution equal to 0.5 cm^{-1}), with an argon–ion laser (λ = 514.5 nm) and a metallographic microscope produced by LEICA® (Rome, Italy). The laser beam was focused on the sample with 15 mW

of excitation power. The spectra were acquired for ten accumulations of 100 s and repeated on five different points.

Then an average of the Raman spectra was obtained and studied. The experimental data were processed by the software produced by Microcal Origin Professional®.

3. Results and Discussion

3.1. ED-XRF Analysis

First of all, a visual examination of the colour of the statue's patinas was carried out: the patinas are mainly dark gray, brown, green, and black.

A preliminary reconnaissance analysis of the statue's surface was performed based on a set of limited, but representative, surface measurements to understand the elemental composition of the patinas. To achieve this purpose, a portable energy-dispersive X-ray fluorescence instrument was used.

Table 2 provides a brief description of each measuring point of the bronze statue and summarizes the experimental results of the ED-XRF analysis obtained before the restoration. It is important to underline that the values reported in Table 2 are surface ED-XRF semi-quantitative values, and they are not true quantitative concentrations of bulk alloy or patina.

Table 2. Brief description of the analysed samples and mean elemental compositions obtained by using ED-XRF before the restoration.

N.	Description	Cu	Zn	Pb	Cl	Fe	Sn	S
		(wt %)						
01	Face	59.0	8.4	<D.L.	3.3	2.3	<D.L.	<D.L.
02	Neck	65.5	9.1	2.5	3.7	4.3	<D.L.	<D.L.
03	Right shoulders	48.0	1.9	3.5	0.9	3.8	17.4	<D.L.
04	Right arm, above	61.5	6.3	3.0	1.8	6.0	7.9	<D.L.
05	Right arm, below	59.5	3.7	2.5	4.0	3.5	<D.L.	<D.L.
06	Right arm, welding	72.0	3.5	<D.L.	2.6	1.5	3.6	<D.L.
07	Left shoulders	55.5	4.9	2.5	2.9	5.1	<D.L.	<D.L.
08	Left arm, above	58.0	2.3	<D.L.	3.2	3.9	<D.L.	2.5
09	Left shoulder blade	59.5	6.6	3.5	3.0	2.9	<D.L.	3.0
10	Right shoulder blade	62.0	5.6	3.0	1.7	2.5	2.9	4.5
11	Left chest	58.5	6.8	2.0	4.5	3.5	<D.L.	<D.L.
12	Left chest, green	53.0	5.7	2.5	1.3	2.6	12.7	4.0
13	Left calf, green	47.0	9.5	<D.L.	2.3	3.0	<D.L.	<D.L.
14	Left calf, black	50.5	8.0	<D.L.	3.7	2.6	<D.L.	<D.L.
15	Left leg, calf	54.0	7.4	2.5	2.1	1.8	4.0	<D.L.
16	Left leg, calf	54.4	9.3	2.5	1.5	2.2	6.6	1.5
17	Left cloak	58.5	10.0	2.0	4.5	2.5	<D.L.	<D.L.
18	Left knee, green	76.0	4.1	<D.L.	6.7	1.2	<D.L.	<D.L.
19	Left knee, black	61.5	5.5	<D.L.	4.6	2.1	<D.L.	<D.L.
20	Base	68.0	5.9	2.5	3.9	2.5	<D.L.	2.5
21	Right foot	67.0	3.3	2.0	5.3	3.0	<D.L.	<D.L.
Standard deviation		±0.5	±0.3	±0.5	±0.3	±0.3	±0.5	±0.5
Detection limit (D.L.)		0.3	0.5	2.0	0.5	0.3	2.5	1.0

The values for the detection limit were determined in agreement with the methods described in Cesareo et al., 2007 [36]. These values, all reported in wt %, for copper, zinc, lead, chlorine, iron, tin and sulphur, are equal, respectively, to 0.3, 0.5, 2.0, 0.5, 0.3, 2.5 and 1.0.

Experimental data demonstrated that all the points analysed contain copper, zinc, chlorine and iron, whereas lead was contained in 14 of 21 areas, tin was contained in seven of 21 areas and sulphur was contained in six of 21 areas.

The concentration of copper in most cases (17 of 21 areas) varies from 50 to 70 wt %; two areas (n. 06 and n. 18) showed concentrations higher than 70 wt % and only two areas showed concentrations lower than 50 wt % (n. 03 and n. 13). This demonstrates that the copper content in the patina is high. In particular, the minimum, maximum, and mean values are 47.0 wt %, 76.0 wt % and 59.5 wt %, respectively.

The constant presence of zinc, typically greater than 1.9 wt %, less than 10 wt % and averaging (6.1 ± 2.0) wt %, might suggest that zinc was probably present in the alloy, but it could also be a corrosion product.

Lead is present in 14 of the 21 investigated areas. The minimum, maximum, and mean values are 2.0 wt %, 3.5 wt % and 2.6 wt %, respectively. The lead concentrations for points n. 11, n. 17 and n. 21 are each equal to 2.0 wt %. Since these values are close to the detection limit (2.0 wt %), it is important to emphasize that they should be considered as the qualitative presence of trace amounts rather than a reliable quantitative concentration. Similar considerations apply to measurements n. 10 for tin (2.9 ± 0.5 wt %; D.L. = 2.5 wt %) and n. 16 for sulphur (1.5 ± 0.5 wt %; D.L. = 1.0 wt %).

Considering the concentrations of copper, lead and zinc obtained by using ED-XRF, the analysed patinas show a relatively homogeneous chemical composition. Figure 5 shows a ternary graph with the concentrations of copper, lead and zinc. The result obtained shows how the samples are grouped into a large cluster and this is probably due to a homogeneous exposure over the years.

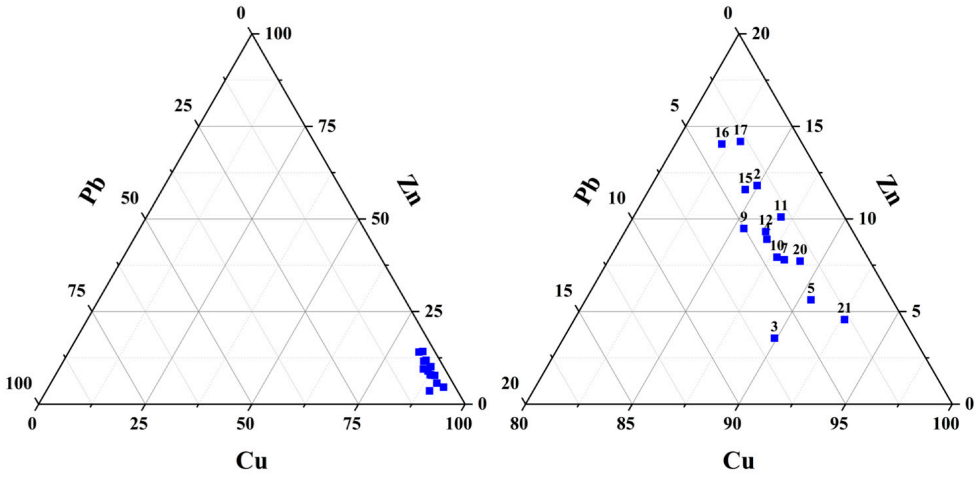

Figure 5. Triangular diagram with concentrations of copper, lead and zinc, obtained by using ED-XRF. The graph on the right shows an enlargement with the names of the samples.

Tin was detected in seven of 21 regions: in outdoor metal alloys, tin is present as SnO_2, a stable and extremely thin patina that can then be covered by other corrosion compounds of the alloy [37]. It is observed that the presence of tin is typically associated with relatively low concentrations of chlorine (regions 3, 4, 6, 10, 12, 15 and 16, and especially for regions n. 3 and n. 12), and consequently, in regions with high chlorine concentrations (for example, 5, 11, 17, 18, 19 and 21), tin is below the detection limit. This demonstrates that the copper chloride patina covers any existing SnO_2 patina.

Moreover, the elements that characterize the depositions, such as iron and lead, are equivalent in the different regions monitored. This could lead to the hypothesis that they were exposed to similar microclimatic and environmental conditions for the same period. In particular, we specify that in Brindisi, air pollution is mainly due to vehicular traffic and

that the natural components of the atmospheric particulate matter are mostly attributable to marine aerosol and to Saharan dust phenomena [38]. However, it is very important to consider that the iron can also derive from several internal and intrinsic sources related to the construction of the statue itself such as, for example, alloy impurities, casting cores and molds naturally rich in iron oxides, and internal iron armature.

As previously mentioned, the artifact is located 300 m from the sea and therefore it has always been exposed to marine aerosols. In fact, the experimental results show that the entire surface of the artifact is characterized by the presence of chlorine, with concentrations ranging from 0.9 wt % to 6.7% wt. Furthermore, the chlorine distribution does not depend on the orientation of the statue with respect to the cardinal points.

As already observed, the lowest chlorine concentrations are recorded in the regions where tin is present (regions 3, 4, 6, 10, 12, 15 and 16): in these regions the average chlorine concentration is equal to (1.7 $\pm$ 0.5) wt %, compared to an average of (4.0 $\pm$ 1.1) wt % in the remaining regions.

It is also observed that the regions most exposed to water erosion (regions 13, 7, 9, 8, 1, 2 and 14) are characterised by slightly lower chlorine concentrations (3.2 $\pm$ 0.5) wt %, compared to regions less exposed to water erosion (regions 18, 21, 19, 17, 5 and 20) in which the average value is equal to (4.8 $\pm$ 1.0) wt %. This suggests that marine aerosol, over the years, has deposited chlorine on the surface of the artifact regardless of wind direction and that rain has then partially removed the chlorine in the regions where the washing away effect was more evident.

Iron is present in all the patinas analysed. The minimum, maximum, and mean values are 1.2 wt %, 6.0 wt % and 3.0 wt %, respectively.

Sulphur is present in only six of the 21 total areas analysed. The minimum, maximum, and mean values are 1.5 wt %, 4.5 wt % and 3.0 wt %, respectively.

Our experimental results are in agreement with those obtained in other studies of patinas on outdoor bronze manufact using different analytical techniques [5,16,39], although it is not possible to make an in-depth comparison since very often the composition of the alloy is unknown, and the exposure times and even the atmospheric conditions are not perfectly comparable.

3.2. XRD Analysis

XRD analysis was performed to determine the chemical composition of a patina sampled from an area of the statue corresponding to the left leg. This area was characterised by the presence of a dark-grey and green patina. Since the analyses were performed on a single sample, we would like to emphasize that the XRD results represent a localized micro-environment and cannot be extrapolated to characterize the surface chemistry of the entire monument.

The XRD spectrum (Figure 6) shows that the sample consisted mainly of cuprite (Cu_2O), atacamite ($Cu_2Cl(OH)_3$), clinoatacamite ($Cu_2Cl(OH)_3$), zincite (ZnO), brochantite ($Cu_4SO_4(OH)_6$) and traces of carbon and calcite ($CaCO_3$). The calcite, detected in low concentration in XRD, is probably due to particulate deposits, which are very frequent in the studied area. Cuprite and zincite are compounds that can be detected in the patinas of more modern bronze statues [12]. The artefact was made of a copper alloy containing zinc. The carbon may probably be due to deposition of atmospheric particulate matter that did not chemically react with the artifact. The atacamite, clinoatacamite and brochantite represent the artifact's interaction with the surrounding environment [40–42]. The brochantite derives from interaction with sulphur oxides present in the atmosphere, while the atacamite and clinoatacamite derive from interaction with marine aerosols.

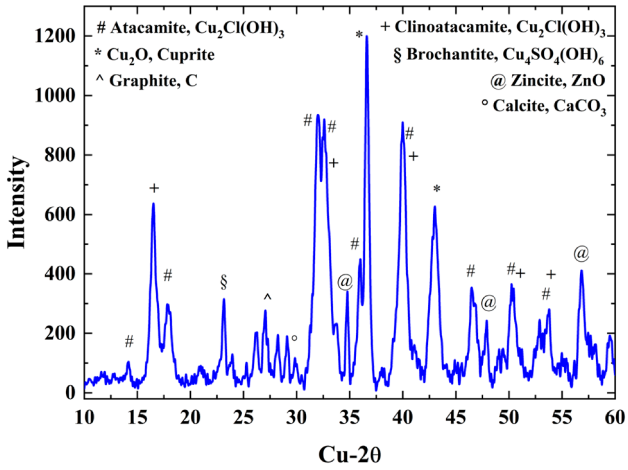

Figure 6. XRD spectrum of a patina sampled from the left leg of the statue.

3.3. Raman Spectroscopy

Raman analysis was performed on the same sample used for the XRD analysis. Since the analyses were achieved on a single sample, we would like to underline that the Raman results represent a localized micro-environment and cannot be extrapolated to characterize the surface of the entire manufact. Raman analysis of the sampled powder (Figure 7) confirmed the presence of calcite (155, 285, 715 and 1085 cm^{-1}) [43], atacamite (220, 415, 510, 635, 810, 905 and 980 cm^{-1}) [44] and brochantite (120, 140, 200, 242, 318, 390, 420, 450, 485, 506, 595, 609, 622, 910 and 975 cm^{-1}) [45], compounds also determined by X-ray diffraction. Our attention was focused on the presence of carbonaceous material. Figure 8 shows the Raman spectrum, which has the following signals: 1350, 1580, 2700 and 2931 cm^{-1}. According to the data reported in the scientific literature, all signals are attributable to carbon deposits [46,47].

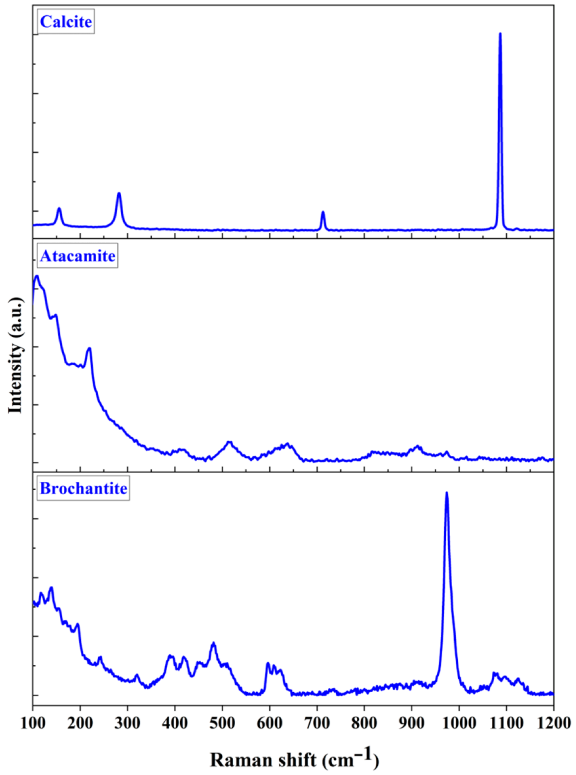

Figure 7. Raman spectra of calcite, atacamite and brochantite determined in the patina sampled from the left leg of the statue.

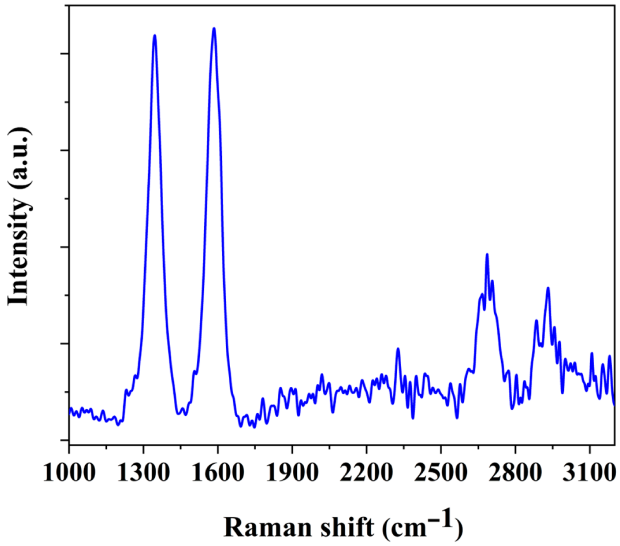

Figure 8. Raman spectrum of the presence of carbonaceous material in the patina sampled from the left leg of the statue.

The signal at 1350 cm^{-1} is known as "D band" (disorder band graphitic) and it indicates the structural defects in the graphite lattice. The signal at 1580 cm^{-1} is known as the "G band" (graphitic band) and it represents the in-plane vibrations of sp^2 hybridized carbon atoms. The signal at 2700 cm^{-1} is known as "2D or G' band", the overtone of the D band, whereas the signal at 2931 cm^{-1} indicates the C–H stretching and it is crucial since it does not come from pure carbon and it indicates the presence of organic compounds.

Calculating intensity ratios is a fundamental step in Raman spectroscopy, as it allows us to quantify the structural disorder of carbon and the relative concentration of the components. The intensity ratio between the D band and G band (I_D/I_G) is the primary parameter used for characterizing carbonaceous materials. A ratio of 1.0 indicates a highly disordered material, while this ratio would be close to zero in a perfect graphite crystal.

In our study, the intensity ratio I_D/I_G is equal to 1. This value suggests a high degree of structural disorder and it may be due to carbon black, charcoal, or soot from environmental pollution [48].

This result is plausible considering the location the statue has been in over the years.

Moreover, the intensity ratio between the 2D band and G band (I_{2D}/I_G) is another sensitive indicator of doping and electronic structure used to determine the degree of "graphitization" or crystallinity [49]. In the case of high-grade graphite or graphene, this ratio is high. In our case, the ratio is low (equal to 0.38), which is attributable to an amorphous or microcrystalline structure.

Therefore, we can deduce that the analysed deposit may probably be due to pollution caused by vehicular traffic, domestic heating or industrial activities.

4. Conclusions

The patinas of an outdoor bronze statue were studied before restoration. In particular, in situ energy-dispersive X-ray fluorescence analyses were carried out on various areas of the monument to evaluate the chemical composition. The results obtained show relatively uniform distributions of all elements.

Moreover, X-ray diffraction and Raman spectroscopy analyses were carried out on a patina sampled from an area not exposed to water erosion. Since conservation constraints prevent further sampling, the XRD and Raman results concern a single specimen from a sheltered area not subject to leaching. For this reason, we would like to emphasize that the

experimental results represent a localized micro-environment and cannot be extrapolated to characterize the surface chemistry of the entire monument.

The experimental results show that the sample consisted mainly of cuprite, atacamite, clinoatacamite, zincite, brochantite and traces of carbon and calcite.

Regarding chlorine, XRD and Raman analyses revealed the presence of atacamite and clinoatacamite, stable basic copper chlorides.

Paratacamite, an unstable chlorinated compound that can cause degradation, was not detected in the analysed sample within the detection limits of the methods used. However, its presence in other areas of the statue cannot be excluded. This information was crucial for the restorers' subsequent work. Indeed, the restorers considered the absence of corrosive compounds determined during the analyses performed. This specifically guided subsequent interventions.

This methodological approach allowed us to determine the chemical composition of the patinas and the information obtained was provided to the restorers for their restoration work on the monument. Therefore, in principle, this method of analysis and interpretation of the results may be employed for other study cases.

Author Contributions: Conceptualization, G.B. (Giovanni Buccolieri), A.S., E.P., F.P., G.B. (Gianluca Bozzetti), A.C. and A.B.; methodology, G.B. (Giovanni Buccolieri), A.S., E.P., F.P., G.B. (Gianluca Bozzetti), A.C. and A.B.; validation, G.B. (Giovanni Buccolieri), A.S., E.P., F.P., G.B. (Gianluca Bozzetti), A.C. and A.B.; formal analysis, G.B. (Giovanni Buccolieri), A.S., E.P., F.P., G.B. (Gianluca Bozzetti), A.C. and A.B.; investigation, G.B. (Giovanni Buccolieri), A.S., E.P., F.P., G.B. (Gianluca Bozzetti), A.C. and A.B.; resources, G.B. (Giovanni Buccolieri), A.S., E.P., F.P., G.B. (Gianluca Bozzetti), A.C. and A.B.; data curation, G.B. (Giovanni Buccolieri), A.S., E.P., F.P., G.B. (Gianluca Bozzetti), A.C. and A.B.; writing—original draft preparation, G.B. (Giovanni Buccolieri), A.S., E.P., F.P., G.B. (Gianluca Bozzetti), A.C. and A.B.; writing—review and editing, G.B. (Giovanni Buccolieri), A.S., E.P., F.P., G.B. (Gianluca Bozzetti), A.C. and A.B. All authors have read and agreed to the published version of the manuscript.

Funding: This research received no external funding.

Data Availability Statement: The data are contained within the article.

Acknowledgments: The authors thank Massimo Luggeri of the University of Salento, who has contributed to improving the quality of the figures.

Conflicts of Interest: Author Elisabetta Palmiero is employed by Colaci Emilio Impianti e Restauri. The company had no role in the design of the study; in the collection, analyses, or interpretation of data; in the writing of the manuscript; or in the decision to publish the results. The remaining authors declare no conflicts of interest.

References

1. Liu, Y.; Shen, J.; Yin, Y.; Hu, B.; Song, L. Multidimensional Exploration in Bronze Restorative Conservation under the Synergistic Perspective of Chemistry and Art: A Systematic Review. *npj Herit. Sci.* **2025**, *13*, 646. [CrossRef]
2. Kwon, H.; Cho, N. In-Situ Non Destructive Investigation of Contemporary Outdoor Bronze Sculptures. *Herit. Sci.* **2024**, *12*, 167. [CrossRef]
3. Saleh, S.M.; El-Badry, A.E.-H.A.; Abdel-karim, A.M. Evaluation of the Corrosion Resistance of Bronze Patina or/and Protective Coating on the Surface of the Archaeological Coins. *Sci. Rep.* **2025**, *15*, 2361. [CrossRef] [PubMed]
4. Petiti, C.; Toniolo, L.; Berti, L.; Goidanich, S. Artistic and Laboratory Patinas on Copper and Bronze Surfaces. *Appl. Sci.* **2023**, *13*, 11873. [CrossRef]
5. Petitmangin, A.; Chabas, A.; Blanc, C.; Remusat, L.; Verdier-Paoletti, M.; Bellot-Gurlet, L.; Pires-Brazuna, R.; Alfaro, S.; Nowak, S. Atmospheric Corrosion of Bell Bronze in an Urban Environment: Its Microinfiltration Properties and the Impact on Corrosion Evolution. *Eur. Phys. J. Plus* **2025**, *140*, 969. [CrossRef]
6. Li, H.; Zhang, Z.; Guo, H.; Ren, C.; Liu, C.; Xiang, L. Recent Progress on Corrosion Behavior, Mechanism, and Protection Strategies of Bronze Artefacts. *Heritage* **2025**, *8*, 340. [CrossRef]

7. Liu, Y.; Liu, X.; Xu, S.; Liu, X. Progress in Materials for Metallic Cultural Heritage Conservation: Mechanisms, Applications, and Future Perspectives. *Polymers* **2026**, *18*, 1131. [CrossRef] [PubMed]
8. Scott, D.A. *Copper and Bronze in Art: Corrosion, Colorants, Conservation*; Getty Conservation Institute: Los Angeles, CA, USA, 2003; ISBN 978-0-89236-638-5.
9. Kosec, T.; Leban, M.B.; Ropret, P.; Finšgar, M. The Impact of Urban Rain on the Changes of Bare and Artificially Patinated Bronze during 9-Year Exposure. *Environ. Sci. Pollut. Res.* **2024**, *31*, 31925–31941. [CrossRef] [PubMed]
10. Keheyan, Y.; Lanterna, G. Micro-Stratigraphical Investigation on Corrosion Layers in Ancient Bronze Artefacts of Urartian Period by Scanning Electron Microscopy, Energy-Dispersive Spectrometry, and Optical Microscopy. *Heritage* **2021**, *4*, 2526–2543. [CrossRef]
11. Livingston, R.A. Acid Rain Attack on Outdoor Sculpture in Perspective. *Atmos. Environ.* **2016**, *146*, 332–345. [CrossRef]
12. Kwon, H.; Cho, N. Corrosion Behaviors of Outdoor Bronze Sculptures in an Urban–Industrial Environment: Corrosion Experiment on Artificial Sulfide Patina. *Metals* **2023**, *13*, 1101. [CrossRef]
13. Fan, X.; Freestone, I.C. Occurrence of Phosphatic Corrosion Products on Bronze Swords of the Warring States Period Buried at Lijiaba Site in Chongqing, China. *Herit. Sci.* **2017**, *5*, 48. [CrossRef]
14. Masi, G.; Esvan, J.; Josse, C.; Chiavari, C.; Bernardi, E.; Martini, C.; Bignozzi, M.C.; Gartner, N.; Kosec, T.; Robbiola, L. Characterization of Typical Patinas Simulating Bronze Corrosion in Outdoor Conditions. *Mater. Chem. Phys.* **2017**, *200*, 308–321. [CrossRef]
15. Papadopoulou, O.; Delagrammatikas, M.; Vassiliou, P.; Grassini, S.; Angelini, E.; Gouda, V. Surface and Interface Investigation of Electrochemically Induced Corrosion on a Quaternary Bronze. *Surf. Interface Anal.* **2014**, *46*, 771–775. [CrossRef]
16. Alexander Schröder, S.; Costantini, I.; Etxebarria, I.; Manuel Madariaga, J.; Arana, G. Assessment of Marine and Urban-Industrial Environmental Impact on Stone Acting as the Base of a Quaternary Bronze Sculpture. *Microchem. J.* **2024**, *204*, 111187. [CrossRef]
17. Quaranta, M.; Catelli, E.; Prati, S.; Sciutto, G.; Mazzeo, R. Chinese Archaeological Artefacts: Microstructure and Corrosion Behaviour of High-Leaded Bronzes. *J. Cult. Herit.* **2014**, *15*, 283–291. [CrossRef]
18. Buravlev, I.Y.; Balagurova, A.V.; Shashurin, D.A.; Ivanov, N.P.; Nikitin, Y.G. A Study of the Technological Features of Bronze Anthropomorphic Sculpture Production from the Jin Dynasty (1115–1234 AD) from the Collection of the IHAE FEB RAS. *Heritage* **2026**, *9*, 33. [CrossRef]
19. Pellis, G.; Caldera, F.; Trotta, F.; Biazioli De Oliveira, T.; Rizzi, P.; Poli, T.; Scalarone, D. Enhancing Permanence of Corrosion Inhibitors Within Acrylic Protective Coatings for Outdoor Bronze Using Green Nanocontainers. *Molecules* **2024**, *29*, 5702. [CrossRef] [PubMed]
20. Michalopoulou, V.; Adam-Veleni, P.; Karapanagiotis, I. A Small Bronze Statue from the Archaeological Museum of Thessaloniki; Exploring Its Authenticity. *STAR Sci. Technol. Archaeol. Res.* **2017**, *3*, 303–313. [CrossRef]
21. Orsilli, J.; Caglio, S. Combined Scanned Macro X-Ray Fluorescence and Reflectance Spectroscopy Mapping on Corroded Ancient Bronzes. *Minerals* **2024**, *14*, 192. [CrossRef]
22. Caridi, F.; Paladini, G.; Faenza, P.; Crupi, V.; Majolino, D.; Venuti, V. X-Ray Fluorescence and μ-Raman Analysis of Bronze Sculptures by Giuseppe Renda. *Acta IMEKO* **2024**, *13*, 1–5. [CrossRef]
23. Mazzeo, R.; Prati, S.; Quaranta, M.; Sciutto, G. An Overview of Analytical Techniques and Methods for the Study and Preservation of Artistic and Archaeological Bronzes. *Mediterr. Arhaeology Archaeom.* **2012**, *12*, 261–271.
24. Buccolieri, G.; Buccolieri, A.; Donati, P.; Marabelli, M.; Castellano, A. Portable EDXRF Investigation of the Patinas on the Riace Bronzes. *Nucl. Instrum. Methods Phys. Res. Sect. B Beam Interact. Mater. At.* **2015**, *343*, 101–109. [CrossRef]
25. Wood, J.R.; Liu, Y. A Multivariate Approach to Investigate Metallurgical Technology: The Case of the Chinese Ritual Bronzes. *J. Archaeol. Method. Theory* **2023**, *30*, 707–756. [CrossRef]
26. Porcaro, M.; Lins, S.; Depalmas, A.; Anzalone, R.M.; Iannaccone, R.; Brunetti, A. Characterization of a Unique Nuragic Bronze Navicella with a Combination of X-Ray Fluorescence Spectrometry and Monte Carlo Simulation. *Materials* **2023**, *16*, 7345. [CrossRef] [PubMed]
27. Boccaccini, F.; Riccucci, C.; Messina, E.; Pascucci, M.; Bosi, F.; Chelazzi, D.; Guaragnone, T.; Baglioni, P.; Ingo, G.M.; Di Carlo, G. Reproducing Bronze Archaeological Patinas through Intentional Burial: A Comparison between Short- and Long-Term Interactions with Soil. *Heliyon* **2023**, *9*, e19626. [CrossRef] [PubMed]
28. Gianicolo, E.A.L.; Bruni, A.; Mangia, C.; Cervino, M.; Vigotti, M.A. Acute Effects of Urban and Industrial Pollution in a Government-Designated "Environmental Risk Area": The Case of Brindisi, Italy. *Int. J. Environ. Health Res.* **2013**, *23*, 446–460. [CrossRef] [PubMed]
29. Donateo, A.; Gregoris, E.; Gambaro, A.; Merico, E.; Giua, R.; Nocioni, A.; Contini, D. Contribution of Harbour Activities and Ship Traffic to PM2.5, Particle Number Concentrations and PAHs in a Port City of the Mediterranean Sea (Italy). *Environ. Sci. Pollut. Res.* **2014**, *21*, 9415–9429. [CrossRef] [PubMed]
30. Buccolieri, G.; Serra, A.; Carbone, G.G.; Iacobellis, V.N.; Castellano, A.; Calcagnile, L.; Buccolieri, A. In Situ Investigation of the Medieval Copper Alloy Door in Troia (Southern Italy). *Heritage* **2023**, *6*, 2688–2700. [CrossRef]

31. Bertin, E.P. *Introduction to X-Ray Spectrometric Analysis*; Springer: Boston, MA, USA, 1978; ISBN 978-0-306-31091-1.
32. Uhlig, S.; Möckel, R.; Pleßow, A. Quantitative Analysis of Sulphides and Sulphates by WD-XRF: Capability and Constraints. *X-Ray Spectrom.* **2016**, *45*, 133–137. [CrossRef]
33. Babos, D.V.; Costa, V.C.; Pereira-Filho, E.R. Wavelength Dispersive X-Ray Fluorescence (WD-XRF) Applied to Speciation of Sulphur in Mineral Supplement for Cattle: Evaluation of the Chemical and Matrix Effects. *Microchem. J.* **2019**, *147*, 628–634. [CrossRef]
34. Sitko, R. Quantitative X-Ray Fluorescence Analysis of Samples of Less than 'Infinite Thickness': Difficulties and Possibilities. *Spectrochim. Acta Part. B At. Spectrosc.* **2009**, *64*, 1161–1172. [CrossRef]
35. Orsilli, J.; Migliori, A.; Padilla-Alvarez, R.; Martini, M.; Galli, A. AR-XRF Measurements and Data Treatment for the Evaluation of Gilding Samples of Cultural Heritage. *J. Anal. At. Spectrom.* **2023**, *38*, 174–185. [CrossRef]
36. Cesareo, R.; Ferretti, M.; Gigante, G.E.; Guida, G.; Moioli, P.; Ridolfi, S.; Roldán Garcia, C. The Use of a European Coinage Alloy to Compare the Detection Limits of Mobile XRF Systems. A Feasibility Study. *X-Ray Spectrom.* **2007**, *36*, 167–172. [CrossRef]
37. Jiang, X.; Zhang, J.; Huang, F.; Xie, H.; Li, Q.; Fang, C. A Mechanism Study of Type i Corrosion on the Surface of Ancient Tin Rich Bronzes. *Herit. Sci.* **2024**, *12*, 349. [CrossRef]
38. Cesari, D.; Genga, A.; Ielpo, P.; Siciliano, M.; Mascolo, G.; Grasso, F.M.; Contini, D. Source Apportionment of PM 2.5 in the Harbour–Industrial Area of Brindisi (Italy): Identification and Estimation of the Contribution of in-Port Ship Emissions. *Sci. Total Environ.* **2014**, *497–498*, 392–400. [CrossRef] [PubMed]
39. Caridi, F.; Mancini, S.; Paladini, G.; Faenza, P.; Crupi, V.; Venuti, V.; Majolino, D. XRF Investigation of the Monument to the Fallen of the Great War by Francesco Jerace in San Ferdinando (Reggio Calabria, Italy). In *Proceedings of the 2022 IMEKO TC4 International Conference on Metrology for Archaeology and Cultural Heritage*; IMEKO: Rome, Italy, 2023; pp. 857–861.
40. Nord, A.G.; Tronner, K.; Boyce, A.J. Atmospheric Bronze and Copper Corrosion as an Environmental Indicator. A Study Based on Chemical and Sulphur Isotope Data. *Water Air Soil. Pollut.* **2001**, *127*, 193–204. [CrossRef]
41. Sequeira, C.A.C. Copper and Copper Alloys. In *Uhlig's Corrosion Handbook*; Revie, R.W., Ed.; Wiley: Hoboken, NJ, USA, 2011; pp. 757–785, ISBN 978-0-470-08032-0.
42. Odnevall Wallinder, I.; Zhang, X.; Goidanich, S.; Le Bozec, N.; Herting, G.; Leygraf, C. Corrosion and Runoff Rates of Cu and Three Cu-Alloys in Marine Environments with Increasing Chloride Deposition Rate. *Sci. Total Environ.* **2014**, *472*, 681–694. [CrossRef] [PubMed]
43. Shen, Y.; Zhang, G.; Zhou, X. Identification of an Unusual Pale Green Material on the Surface of an Ancient Chinese Bronze Vessel and Application of Laser Cleaning to Its Removal. *Herit. Sci.* **2023**, *11*, 87. [CrossRef]
44. Porcu, D.; Innocenti, S.; Striova, J.; Carretti, E.; Fontana, R. Mapping Bronze Disease Onset by Multispectral Reflectography. *Minerals* **2025**, *15*, 252. [CrossRef]
45. Coccato, A.; Bersani, D.; Coudray, A.; Sanyova, J.; Moens, L.; Vandenabeele, P. Raman Spectroscopy of Green Minerals and Reaction Products with an Application in Cultural Heritage Research. *J. Raman Spectrosc.* **2016**, *47*, 1429–1443. [CrossRef]
46. Catelani, T.; Pratesi, G.; Zoppi, M. Raman Characterization of Ambient Airborne Soot and Associated Mineral Phases. *Aerosol Sci. Technol.* **2014**, *48*, 13–21. [CrossRef]
47. Escribano, R.; Sloan, J.J.; Siddique, N.; Sze, N.; Dudev, T. Raman Spectroscopy of Carbon-Containing Particles. *Vib. Spectrosc.* **2001**, *26*, 179–186. [CrossRef]
48. Zioła, N.; Banasik, K.; Jabłońska, M.; Janeczek, J.; Błaszczak, B.; Klejnowski, K.; Mathews, B. Seasonality of the Airborne Ambient Soot Predominant Emission Sources Determined by Raman Microspectroscopy and Thermo-Optical Method. *Atmosphere* **2021**, *12*, 768. [CrossRef]
49. Madito, M.J. Revisiting the Raman Disorder Band in Graphene-Based Materials: A Critical Review. *Vib. Spectrosc.* **2025**, *139*, 103814. [CrossRef]